A computational protocol to predict anti-Kasha emissions: the case of azulene derivatives

Koen Veys and Daniel Escudero

Quantum Chemistry and Physical Chemistry Section, Department of Chemistry, KU Leuven, Celestijnenlaan 200f, 3001 Leuven

KEYWORDS

Time dependent density function theory, ADC(2), azulene derivatives, thermal vibration correlation function, anti-Kasha photoluminescence.

ABSTRACT

In this contribution we present a computational protocol to predict anti-Kasha photoluminescence. The herein developed protocol is based on state-of-the-art quantum chemical calculations and excited state decay rate theories (i.e., thermal vibration correlation function formalism), along with appropriate kinetic models which include all relevant electronic states. This protocol is validated for a series of azulene derivatives. For this series, we have computed absorption and emission spectra for both their first and second excited states, their radiative and non-radiative rates as well as fluorescence yields from the two different excited states. All the studied azulene derivatives are predicted to exclusively display anomalous anti-Kasha S_2 emission. A quantitative agreement for

the herein computed excited state spectra, lifetimes and fluorescence quantum yields is obtained with respect to the experimental values. Given the increasing interest on anti-Kasha emitters, we foresee that the herein developed computational protocol can be used to pre-screen dyes with the desired aforementioned anomalous photoluminescence properties.

INTRODUCTION

Photochemistry and photochemical reactivity are often governed by the lowest excited states of molecular systems (S_1 and/or T_1). In this regard, Michael Kasha stated in the 1950's that "the emitting electronic level of a given multiplicity is the lowest excited level of that multiplicity", known as Kasha's rule.[1] This initial formulation was later extended as "polyatomic molecular entities react with appreciable yield only from the lowest excited state of a given multiplicity".[2,3] Certainly, rules are not laws, and thanks to the advances in both experimental and computational techniques able to track the excited state dynamics of molecular systems at different timescales, violations of Kasha's rule are found more and more often in the literature.[4–6] To his credit, Kasha already described an exception to his own rule for the azulene molecule, which shows fluorescence from its second excited state (S_2) instead of the expected Kasha-like fluorescence from S_1.[7] Turro and others[8] described during the 1970's many other molecular systems behaving in an anti-Kasha manner (and not only limited to an anomalous S_2 emission). These findings contributed to put on firmer grounds the early discoveries by Kasha. In 2012, Itoh classified anti-Kasha events according to their different mechanisms.[9] More in detail, Itoh differentiates between thermally-equilibrated and non-thermally-equilibrated scenarios.[9] Indeed, photochemistry is all about competing deactivation channels, and thus, the kinetics of the forward and reverse processes for multiple

excited states have to be concomitantly considered. The final outcome of the photochemical reactions depend on the intricate interplay of internal conversion, vibrational relaxation, and other radiative and non-radiative processes leading to the recovery of the ground state. For instance, the anti-Kasha S_2 emission in azulene can be understood in terms of the very large gap between the S_2 and S_1 levels, and thus the radiative emission from S_2 competes with the internal conversion from S_2 to S_1 (leading to a non-thermally equilibrated scenario between S_2 and S_1). Often, different mechanisms are possible and in principle, one could fit the measured multiexponential decays considering different decay pathways and their kinetics. Therefore, in the latter cases it might be difficult to track the underlying processes with time-resolved experimental techniques.[10] This is for instance the case of diphenyl polyenes, where emission from S_2 takes place as a consequence of the slow internal conversion between S_2 and S_1 but also because of the thermal population of S_2 from S_1.[11] Dual and multiple anti-Kasha scenarios have also been described for other systems.[5,12–16]

Despite the strong pieces of evidence for Kasha's rule violations,[4] there is still some controversy within the community concerning some of the systems which have been reported to behave in an anti-Kasha manner.[17] Certainly, impurities or other experimental artefacts may lead to the wrong assignment of anti-Kasha events. That is why theoretical researches could provide a leap in our fundamental understanding of anti-Kasha events. However, up to now, these investigations have remained on a qualitative or semi-quantitative basis only.[18] Therefore, computational protocols able to predict anti-Kasha photochemical processes on a quantitative basis would be very much acknowledged by the community. Photoluminescence processes take place beyond the nanosecond regime. Thus, the modelling of these events is challenging and it is certainly out of reach for non-adiabatic excited state dynamics.[19] An alternative approach consists of combining diverse excited

state decay rate theories with appropriate kinetic models, as e.g., one of us recently showed for a complex kinetic scenario on phosphors.[20] On the other hand, quantitative calculations of the Kasha-like S_1 fluorescence (i.e., vibronic spectra, lifetimes and quantum yields) have been obtained by the group of Shuai for e.g., several polyenes and the free-base porphyrin.[21] Modelling the S_1 fluorescence case is straightforward, since it requires: i) a minimal kinetic model including only S_1 and S_0 and ii) the evaluation of only two decay rate constants recovering S_0 from S_1, namely the radiative (k_r) and the non-radiative (k_{nr}) decay rates. In Ref. 21 the k_r and k_{nr} rates were evaluated with the thermal vibration correlation function (TVCF) rate theory, also developed at Shuai's group, in combination with linear-response time-dependent density functional theory (LR-TD-DFT) calculations for the excited states and DFT calculations for the ground states. Note that small inaccuracies in e.g., the energy gaps, translate exponentially into the k_{nr} values (and cubically into the k_r values), so that ground and excited state energies and associated excited state and vibrational properties need to be calculated accurately in order to yield quantitative results of excited state lifetimes and quantum yields. This is sometimes not evident, since i) obtaining accurate excited state energies and associated properties is difficult, ii) the potential energy surfaces (PES) of ground and excited states may have remarkable distinct features, and iii) the TVCF theory is currently available within a multidimensional harmonic oscillator approximation only. Within this approximation, displacements, distortions and Duschinsky rotation effects (DRE) are included. This formalism has been proven successful for many different molecular materials, including organic molecules and organometallic complexes.[22–26] Furthermore, this formalism was recently used by Shi *et al*. to explain anti-Kasha luminescence in certain biomolecules, although they only computed radiative rates and they omitted the calculations of internal conversion rates.[27] Certainly, the calculation of anti-Kasha scenarios pose significant additional challenges. Firstly, the kinetic

models should be expanded to include at least S_2, S_1 and S_0 and therefore, more decay rate calculations are needed. Secondly, transition dipole moments and non-adiabatic coupling vectors between excited states, i.e. S_2 and S_1, are not strictly attainable with LR-TD-DFT. Thus, in this work, we have devised some strategies to circumvent these problems in order to make feasible the calculation of anti-Kasha scenarios within the TVCF formalism. All in all, we present, for the first time, a computational protocol to predict anti-Kasha luminescence in molecular systems by considering all important radiative and non-radiative rates. As a case study, several azulene derivatives have been studied, for which we quantitatively calculate spectra, lifetimes and photoluminescence yields from both S_2 and S_1.

Although much research has already been performed to explore the anomalous emission in azulene derivatives, these molecules are still used as a building block to promote anti-Kasha emission.[16,28–30] On top of that, due to its permanent dipole and its ease for yielding chemical substitutions, tailored-made azulene derivatives are promising candidates for their use in organic field effect transistors and solar cells.[31,32] Extensive and exhaustive experimental data on the photophysical properties of azulene derivatives are available in the literature,[33,34] so that these molecules offer the perfect platform to test the validity of our approximations and will permit us to understand and rationalize the observed trends in the excited state lifetimes and quantum yields of the series of azulene derivatives. More in detail, the following substituted azulene derivatives are investigated in this work: azulene (**1a**), guaiazulene or 1,4-dimethyl-7-isopropylazulene (**1b**), 1,3-dichloro- (**1c**), 1,3-dibromo- (**1d**) and 5,6-dichloroazulene (**1e**) (see **Figure 1**).

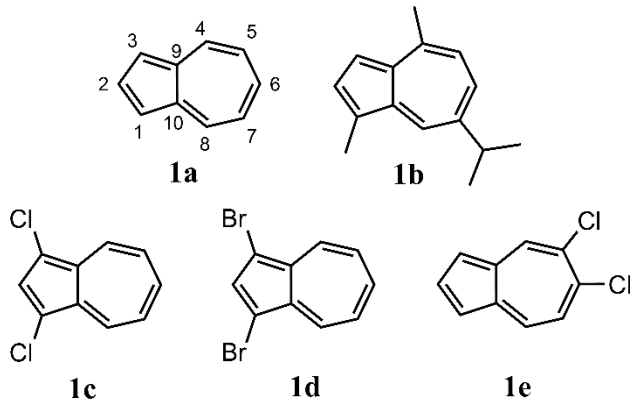

Figure 1. Chemical structures of the azulene derivatives **1a-e**, together with the numbering of the carbon atoms.

COMPUTATIONAL DETAILS

All geometry optimizations and frequency calculations were carried out without symmetry constraints, using density functional theory (DFT)[35–37] for ground states and LR-TD-DFT[38,39] for the first two singlet excited states, S_1 and S_2, using the PBE0 functional[40–42] in combination with the 6-31G(d) basis sets.[43–52] The geometry optimizations were performed in the gas phase. Single point energy calculations were performed on these geometries using the second order algebraic diagrammatic construction (ADC(2)) method[53] in combination with the def2-TZVP basis sets,[54] with the goal of obtaining accurate adiabatic energy differences (ΔE_{ad}) and transition dipole moments (TDMs), the latter being evaluated using the computed relaxed properties.[55] The excited state decay rates and UV-Vis absorption and emission spectra were calculated using the TVCF formalism, as implemented in the MOMAP-2019B program package.[56–58] The TVCF makes use of a multidimensional harmonic oscillator level, where displacements, distortions, DRE and Herzberg-Teller (HT) effects can be considered. In addition, it makes use of the fast Fourier

transform technique, which is applied to save computing time and to improve the efficiency of e.g., emission spectra and rate calculations. In this work, all rate and S_1 spectra calculations include DRE. The HT contributions are only relevant in the case of dipole-forbidden transitions and weakly dipole-allowed transitions. Only for the calculations of the S_2 spectra, both DRE and HT effects were considered.[21] The computed spectra were broadened with a Lorentzian function of 250 cm^{-1}.

The radiative rates, i.e. k_r, were evaluated by integrating the computed light emission spectra. The internal conversion (IC) rates, i.e., k_{ic}, are derived from the combination of Fermi's golden rule and first-order perturbation theory. Here, the Condon approximation was applied and the interaction between the two Born-Oppenheimer states is established by using the non-adiabatic coupling operator. The TVCF formalism was also employed for the k_{ic} calculations. More detailed information about the formulations and implementation of the TVCF formalism as well as the exact k_r and k_{ic} expressions can be found elsewhere.[21,56–58] For the k_{ic} calculations, the convergence of the time-integration was always verified, and it was achieved in all cases by using an integration time of 2000 fs and a timestep of 0.05 fs at a temperature of 298K. In addition, an extra smoothing step in the latter calculations was performed to the reduce the noise (see **Figure S1** in the SI). For the k_{ic} calculations we made use of: i) the PBE0/6-31G(d) (for S_0) and LR-TD-PBE0/6-31G(d) (for S_1 and S_2) frequency calculations and of ii) the adiabatic energy gaps (ΔE_{ad}) obtained with ADC(2)/def2-TZVP, because the latter values are found to be of superior quality than the ones obtained with LR-TD-PBE0/6-31G(d) (see discussion in the results section). Note also that the 0-0 energies, i.e., $E^{0\text{-}0}$, were obtained by correcting the ΔE_{ad} values from ADC(2) with the zero-point energies from the DFT calculations. $E^{0\text{-}0}$ values are directly comparable with the experiments because they correspond to the intersection point between the absorption and emission spectra.

In addition, the electronic TDMs were calculated as follows. The ground-to-excited state TDMs are based on the ADC(2)/def2-TZVP calculations. However, when studying properties between excited states linear response methods are no longer strictly suited. Thus, quadratic response (QR)-TD-DFT[59] was used herein to obtain the TDMs between S_2 and S_1. For these calculations we used the CAM-B3LYP functional[60] in combination with the 6-31G(d) basis set for all elements except bromine, for which the aug-cc-pVDZ[61–64] basis set was used.

Finally, the TVCF calculations also require the calculations of non-adiabatic coupling matrix elements (NACMEs). For the NACMEs between ground and excited states, first-order perturbation theory was applied to compute the non-adiabatic electronic couplings, which requires the evaluation of the transition electric field.[21] Herein, the transition electric field was evaluated with LR-TD-PBE0/6-31G(d) calculations. Conversely, to get the NACMEs between excited states (i.e., S_2 and S_1), linear response methods are again no longer strictly suited. Therefore, in the latter cases the transition electric field was evaluated with configuration interaction singles[65] (i.e., CIS/6-31G(d)) calculations.

All DFT, LR-TD-DFT and CIS calculations were performed with the Gaussian16A03 program package[66], the ADC(2)[67–69] calculations with Turbomole 7.1[70] and the QR-TDDFT calculations with the Dalton program, version 2016.2.[71,72]

RESULTS AND DISCUSSION

Geometries, energetics and related properties.

First we discuss the geometrical parameters of the optimized S_0, S_1 and S_2 geometries of the azulene derivatives. **Figure S2** shows exemplarily the main geometrical parameters for **1a**, in which the central C9-C10 bond distance amounts up to 1.49 Å in the S_0 optimized geometry. This

bond considerably shortens in the S_1 optimized geometry (1.39 Å), while only slightly in the S_2 optimized geometry (1.46 Å). Other bond distances only changed less than 0.05 Å, rendering quite similar geometrical parameters for S_0 and S_2. The trends within the series of azulene derivatives did not vary significantly, with maximum differences of ca. 0.02 Å.

Table 1. Vertical excitation and 0-0 energies (in eV) for the $S_0 \rightarrow S_1$ and $S_0 \rightarrow S_2$ transitions of **1a**-**1e** along with their oscillator strengths (in au) obtained from the TD-PBE0/6-31G(d) and ADC(2)/ def-TZVP (between parentheses) calculations.

	$S_0 \rightarrow S_1$				$S_0 \rightarrow S_2$			
	E_v (eV)[a]	f (au)[b]	E^{0-0} (eV)[c]	Exp. E^{0-0} (eV)[d]	E_v (eV)[a]	f (au)[b]	E^{0-0} (eV)[c]	Exp. E^{0-0} (eV)[d]
1a	2.47[e] (2.24)	0.008 (0.009)	2.04 (1.81)	1.77	3.77 (3.85)	0.002 (0.005)	3.61 (3.66)	3.50
1b	2.34 (2.16)	0.013 (0.015)	1.91 (1.68)	1.64	3.63 (3.69)	0.020 (0.040)	3.44 (3.45)	3.34
1c	2.18 (1.96)	0.008 (0.010)	1.78 (1.55)	1.59	3.60 (3.65)	0.029 (0.058)	3.44 (3.45)	3.35
1d	2.18 (1.97)	0.008 (0.010)	1.78 (1.57)	1.62	3.56 (3.60)	0.033 (0.074)	3.40 (3.40)	3.34
1e	2.36 (2.14)	0.009 (0.010)	1.96 (1.72)	1.71	3.62 (3.69)	0.002 (0.002)	3.46 (3.50)	3.38

[a] Vertical excitation energies, [b] oscillator strengths, [c] 0-0 energies and [d] experimental E^{0-0} values from Ref. 34 in 3-methylpentane.

¡Error! No se encuentra el origen de la referencia. collects the TD-PBE0 and ADC(2) vertical excitation energies (E_v) along with oscillator strengths for both the $S_0 \rightarrow S_1$ and $S_0 \rightarrow S_2$ excitations for **1a**-**1e**. 0-0 energies are also tabulated in **¡Error! No se encuentra el origen de la referencia.**. We recall that the E^{0-0} values are directly comparable with the experimental ones. For S_1, the computed E_v and E^{0-0} values with TD-PBE0 are systematically overestimated by 0.2 eV with respect to the ADC(2) estimates and the E^{0-0} value with the latter method (1.81 eV, see ¡Error! No

se encuentra el origen de la referencia.) shows a very good agreement (within 0.05 eV) with the experimental one (1.77 eV). In the case of S_2, both TDDFT and ADC(2) calculations render rather similar energetic estimates, being both overestimated by up to 0.15 eV with respect to the experimental values. These errors are within the expected range of accuracy for ADC(2) for the excitation energies of organic molecules (ca. 1000 cm^{-1}).[73] High level ab-initio data (CASPT2/6-31G*, using a 10/10 active space) from Murakami *et al*.[74] are also available for the excited states of **1a**. More in detail, the CASPT2 estimates for the E^{0-0} values are 1.66 and 3.67 eV for S_1 and S_2, respectively.[74] Thus, while both CASPT2 and ADC(2) predict the S_2 state within the same 0.15 eV error margin, CASPT2 locates the S_1 state with a larger error than ADC(2). All in all, we conclude that ADC(2) is accurate enough for the excited states of the series of azulene derivatives studied herein and thus the discussion in the following is mainly based on the ADC(2) results. Besides correct absolute values, the experimental trends within the series in the UV-Vis absorption characteristics are also recovered by our calculations. For instance, **1a** possesses the largest E^{0-0} values for both S_1 and S_2, while **1c** has the smallest E^{0-0} value for S_1 and **1d** the smallest E^{0-0} value for S_2. In addition, **1a** possesses the highest E_v values for both S_1 and S_2. The *1,3*-disubstitution of **1a** with electron withdrawing groups (**1c-d**) leads to a red-shift of ca. 0.3 and 0.2 eV for the S_1 and S_2 peaks, respectively; with respect to **1a**. Alike di-substitution on the 5,6 positions (**1e**) leads however to red-shifts of only 0.1 and 0.15 eV for S_1 and S_2, respectively. Guaiazulene (**1b**), bearing methyl substitutions on the 1,4,7 positions, possesses very similar E_v values to those of **1e** for both S_1 and S_2. Finally, the relaxation on the S_1 PES results in a red-shift of ca. 0.4 eV from the vertical point to the S_1 minimum. In the case of the S_2 the red-shift amounts only up to ca. 0.2 eV, in line with the similarities found between the S_0 and S_2 optimized

geometries. This latter trend is similar for all the azulene derivatives regardless of their substitution pattern.

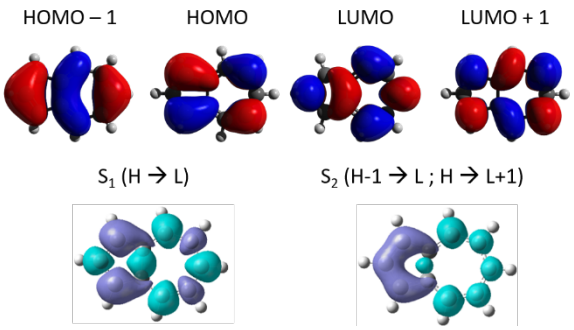

Figure 2. Kohn-Sham frontier molecular orbitals (top) and electron density difference maps for S_1 and S_2 (bottom) of **1a**.

We now turn the discussion to the excited state characters of S_1 and S_2. As commonly found for other polyacenes[75], S_1 consists mainly of a HOMO → LUMO excitation in **1a**-**1e**. On the other hand, S_2 has significant contributions from both HOMO-1 → LUMO and HOMO → LUMO+1. (See the involved frontier molecular orbitals for **1a** and the corresponding electron density difference plots for S_1 and S_2 in **Figure 2**.) The characters of S_1 and S_2 do not vary much regardless of the level of theory used (see **Table S1**) and of the substitution pattern within the **1a**-**e** series (see **Figures S3-S4**). However, **1b**-**d** have a slightly lower (~10%) contribution from the HOMO-1 → LUMO in the S_2. The latter trend results in larger S_2 oscillator strengths for **1b**-**d** (**¡Error! No se encuentra el origen de la referencia.**), while the S_1 oscillator strengths remain alike within the series. Finally, in the electron density difference maps (see **Figure S4**) one can see for **1c-d** that there is some charge transfer away from the halogen atoms at the *1,3*-positions in both S_1 and S_2. However, for **1e**, there is significantly less transfer at the *6*-position in S_2. This is in agreement

with earlier observations, where substituents at even positions have a different effect than those at odd positions.[76]

UV-Vis absorption and emission spectra.

The UV-Vis absorption and emission spectra were computed with the TVCF formalism (see computational details above). The experimental spectra of **1a**-**e** display vibronically resolved S_1 and S_2 absorption bands.[33] As discussed above, only the emission from S_2 occurs experimentally in a considerable yield for all the compounds, while the S_1 emission is negligible. The rationalization of this anti-Kasha photoluminescence is presented in the following subsection. The computed spectra for **1a**, along with the experimental one reported in Ref. 33, are shown in **Figure 3a** (see in **Figure S5** the spectra for **1b**-**e**). The shape of the S_1 calculated absorption spectrum, which includes only the Franck-Condon (FC) contributions, is in very good agreement with the experimental one. As it can be seen in **Figure 3a**, the intensity and positions of all the vibrational features are satisfactorily recovered by the calculations. Conversely, the S_2 absorption spectrum of **1a** was calculated with the FC approximation (see **Figure 3b)** and also including HT contributions (see the total spectra in **Figure 3c**). In **Figure 3b-c** the computed S_2 emission spectra are also displayed for completeness. As it can be seen in **Figure 3b**, the FC contribution alone appears to be inaccurate to predict the correct intensity and positions of the different vibrational peaks of S_2. The vibronic features of the experimental S_2 absorption and emission spectra are only recovered after the inclusion of HT effects (**Figure 3c**). The relevance of HT effects on the S_2 emission of azulene have also been proved by Prlj *et al*.[77] In Ref. 77 they combined a semiclassical approach with *ab initio* calculations to account for the anomalous emission in azulene. HT effects are also relevant for **1c** (see **Figure S5**). Conversely, for **1b**, HT effects are definitely less important. As it can be seen in **Figure S5** the spectra with and without HT are very similar for **1b** and they both

predict a more pronounced 0-0 transition, in agreement with the experimental evidence. Certainly, **1b** has a larger S_2 oscillator strength (see **¡Error! No se encuentra el origen de la referencia.**) than **1a** and **1c**, so that HT contributions become less important for the former compound.

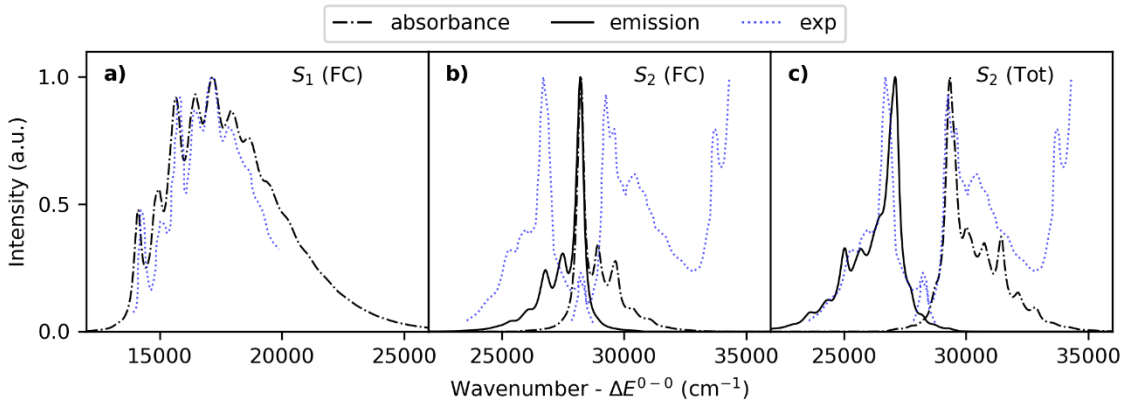

Figure 3. Calculated (black line) and experimental[33] (blue, dotted line) spectra of **1a**. The S_1 absorption is shown in panel **a**, while the S_2 absorption/emission are shown in panels **b** and **c**. In **b**, only the Franck-Condon (FC) contribution is considered in the spectra calculation, while in **c**, the total (Tot) spectrum is used, where also the HT effect is included. The high energy peak in the experimental absorption spectrum in panels **b** and **c** is caused by S_3, which was not considered in the calculations of the spectrum. All spectra were normalized, the calculated spectra were shifted to the experimental 0-0-transition and a broadening factor of 250 cm^{-1} was used.

Kinetic model, radiative and non-radiative rates and fluorescence yields.

We now turn the discussion to the rationalization of the experimentally observed anti-Kasha emission in azulene derivatives.[33,34] Toward this end, we propose a kinetic model which includes the most likely photodeactivation channels after population of the S_2 state, see **Chart 1**.

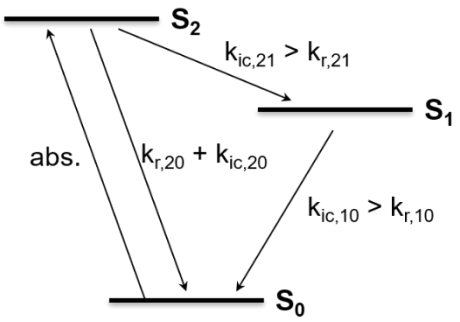

Chart 1. Schematic Jablonski diagram including the competing photodeactivation channels after excitation (abs.) of the S_2 state. Here, k_r denotes the radiative rate, while k_{ic} represents the internal conversion rate, which is the main contribution to the non-radiative rate.

After a molecule absorbs light, there are mainly two possible deactivation pathways: radiative and non-radiative decay. Several non-radiative decay paths are possible, and they all may contribute to the total non-radiative rate, k_{nr}. To unambiguously determine the presence or absence of fluorescence, one should consider all the relevant pathways in the kinetic model, leading to the following, general equation of the fluorescence yield ϕ:

$$\phi = \frac{k_r}{k_r + k_{nr}} = k_r * \tau. \quad (1)$$

Here, the lifetime τ, is the inverse of the sum of all decay rates, both radiative and non-radiative. The k_{nr}. may stand for internal conversion (k_{ic}) and intersystem crossing (k_{isc}) processes; but also for other decays such as e.g., photoreactions. However, for azulene derivatives, intersystem crossing processes among other possible non-radiative decay pathways are not relevant.[34] Thus, they are neglected in our kinetic models. After excitation to the S_2 state, the quantum yield for $S_2 \rightarrow S_0$ fluorescence, i.e., ϕ_{20}, can be written as follows according to the kinetic model of **Chart 1**:

$$\phi_{20} = k_{r,20} * \tau_2 \approx \frac{k_{r,20}}{k_{r,20} + k_{ic,21}}. \quad (2)$$

In Eq. (2), the $S_2 \rightarrow S_0$ internal conversion rate ($k_{ic,20}$) is neglected because it is assumed to be much smaller than $k_{ic,21}$ in view of the S_2-S_1 and S_2-S_0 relative energy gaps. Furthermore, the $S_2 \rightarrow S_1$ fluorescence rate is also neglected because radiative rates depend on the cube of the energy gap, and thus $k_{r,21}$ is also negligible as compared with $k_{r,20}$. These assumptions are later validated in this work.

For the S_1 decay, the expression for the fluorescence yield is more intricate, since the initially populated S_2 state might also decay in a radiative manner to S_0, and thus the direct population of S_1, which occurs only from the non-radiative decay from S_2 to S_1, might not always be the only relevant pathway. Therefore, inclusion of the $S_2 \rightarrow S_1$ rates and of the S_2 lifetime are necessary to obtain an accurate yield. The quantum yield for $S_1 \rightarrow S_0$ fluorescence, i.e., ϕ_{10}, can be written as follows:

$$\phi_{10} = k_{r,10} * \tau_1 * (k_{r,21} + k_{ic,21}) * \tau_2 \,, \tag{3}$$

$$\approx \frac{k_{r,10}}{k_{r,10} + k_{ic,10}} * \frac{k_{ic,21}}{k_{r,20} + k_{ic,21}}, \tag{4}$$

$$\approx \frac{k_{r,10}}{k_{ic,10}}, \tag{5}$$

where the last approximation is only valid if the $S_2 \rightarrow S_1$ and $S_1 \rightarrow S_0$ internal conversions are the main deactivation pathways, making the radiative rates negligible, and the last term of Eq. (4) equal to one.

In **Table 2**, we collect the computed radiative and internal conversion decay rates (see Computational Details) for **1a**-**1e**; along with the fluorescence quantum yield according to expressions (2) and (5). In all cases, both equations (4) and (5) gave the same results, making our approximations for ϕ_{10} valid. In addition, the experimental values reported in Refs. 33, 34, 78 are shown for completeness. One should notice that slightly different values were obtained by different

experimental research groups, and thus they give an estimate of the error margin from the experiments. First, importantly, for all the azulene derivatives only $S_2 \rightarrow S_0$ fluorescence is predicted (see **Table 2**) in a considerable yield. Note that the fluorescence yield from S_2 is at least 1500 times larger than the yield from S_1. These results are in very good agreement with the experiments, where fluorescence from S_1 was not observed.[34]

Table 2. Calculated and experimental radiative rates, non-radiative rates (s^{-1}) and fluorescence yields (%). Experimental values are given between parentheses.

	k_r ($\times 10^7$ s^{-1})[a]		k_{ic} (s^{-1})[a]		ϕ (%)[a]	
	$S_1 \rightarrow S_0$	$S_2 \rightarrow S_0$	$S_1 \rightarrow S_0$	$S_2 \rightarrow S_1$	$S_1 \rightarrow S_0$	$S_2 \rightarrow S_0$
1a	0.16	2.7 (2.3 ± 0.1)[b,c]	1.9×10^{11}	6.3×10^{8} ($5.3\pm1.2\times10^{8}$)[b,c,d]	8.4×10^{-4}	4.3 (3.5 ± 0.4)[b,c]
1b	0.12	1.7 (3.2 ± 0.4)[b,c]	6.7×10^{11}	5.5×10^{9} ($2.1\pm0.1\times10^{9}$)[b,c]	1.8×10^{-4}	0.31 (1.5 ± 0.1)[b,c]
1c	0.15	2.5 (3.6 ± 0.1)[b,c]	7.8×10^{11}	1.7×10^{9} ($7.0\pm1.2\times10^{8}$)[b,c]	1.9×10^{-4}	1.5 (5.0 ± 0.9)[b,c]
1d	0.20	2.7 (3.5)[c]	1.0×10^{12}	3.3×10^{9} (2.9×10^{9})[c]	2.0×10^{-4}	0.82 (1.2)[c]
1e	0.12	1.2 (2.4)[c]	4.6×10^{11}	2.7×10^{9} (9.0×10^{8})[c]	2.6×10^{-4}	0.44 (2.6)[c]

[a]Calculated radiative rates (k_r), non-radiative rates (k_{nr}) and fluorescence yields (ϕ) using the calculated S_2-S_0, S_2-S_1 and S_1-S_0 ADC(2)/def2-TZVP energy gaps. Yields are calculated according to equations (2) and (5). Experimental data are averaged values from ref. 33 (b), ref. 34 (c) and ref. 78 (d), respectively.

Let us first discuss the individual radiative rates for the series of azulene derivatives. One can see that the computed radiative decay rates from S_2 ($k_{r,20}$) agree well with the experimental values, all of them being in the same order of magnitude as the experimental ones. Apart from **1a**, they are systematically slightly underestimated, likely arising from the underestimated computed energy gaps. Also note the discrepancies between the two different sets of experimental results

(e.g., error margin of ca. 0.4×10^7 s^{-1} for **1b**). To validate the approximation made in the derivation of Eq. (2), we also calculated the $k_{r,21}$ values. The latter values are in the order of 10^3 to 10^5, and thus they are indeed negligible as compared to the $k_{ic,21}$ values, which are at least three orders of magnitude larger for **1a**-**1e**.

On the other hand, the non-radiative rates are less straightforward to compare with experiment, since they cannot be measured directly, and they may involve different processes. However, as mentioned before, for the S_2 decay, the experimentally measured non-radiative rate mainly consists of $S_2 \rightarrow S_1$ internal conversion ($k_{ic,21}$). This is indeed supported by our calculations, which predict $k_{ic,20}$ values of the order of $10^2 - 10^5$ s^{-1} (see the computed values in **Table S3**). Therefore, the $S_2 \rightarrow S_0$ IC process is not competitive with the $S_2 \rightarrow S_1$ IC process, because the $k_{ic,21}$ values are in the order of 10^8-10^9 s^{-1}. These results refute a previous experimental hypothesis of the putative role of $S_2 \rightarrow S_0$ IC on contributing to the global non-radiative decay.[34] In this regard, it is interesting to note that for these azulene derivatives the energy gap law for non-radiative rates is not fully met, in agreement with the early observations by Griesser *et al*.[34] This is shown in **¡Error! No se encuentra el origen de la referencia.** and **Table 2**, where it can be clearly seen that some compounds possessing larger S_2-S_1 adiabatic gaps possess unexpectedly larger $k_{ic,21}$ values (e.g., compare **1a** with **1c**). In **Figure 4**, the agreement between the experimental and computed $k_{ic,21}$ values is shown. The computed values using ADC(2) adiabatic energy gaps are shown in light blue while those based on TD-DFT energy gaps are shown in green. One can clearly see that only the $k_{ic,21}$ values based on the ADC(2) calculations yield a quantitative agreement with the experimental results (i.e., within the same order of magnitude). This latter approach is also the only one able to recover all the experimental trends on the $k_{ic,21}$ values within the **1a**-**e** series. Thus, these results highlight on the one hand side the sensitivity of the rate calculations with regards to small

inaccuracies on the computed energy gaps; and on the other hand side they highlight the need to rely on highly correlated calculations, especially for the IC decay rate calculations (the differences are slightly less dramatic for radiative rate calculations, see **Table S2** and **S3**). In a nutshell, the photoluminescence quantum yield calculations presented below are based on the ADC(2) data only.

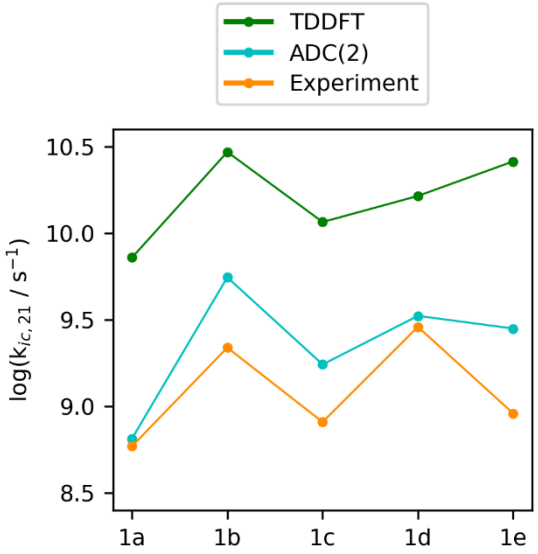

Figure 4. Logarithm of the experimental and calculated (both based on TDDFT and ADC(2) data) $S_2 \rightarrow S_1$ internal conversion decay rates rates.

Let us study first a bit more in detail the computed divergences from the energy gap law within the **1a-e** series and the underlying vibrational modes promoting internal conversion decay. According to the literature,[56,79] the evolution of $\log(k_{ic})$ as a function of the energy gap, can be approximately represented as a downwards parabola, depending on the reorganization energies (REs) between the two involved states. This approximation starts with Fermi's golden-rule, stating that the transition rate depends on the coupling (H) between initial and final state as well as on the Franck-Condon weighted density of states (FCWD) according to following equation:[80]

$$k = \left(\frac{2\pi}{\hbar}\right) H^2 * FCWD. \quad (6)$$

In the high-temperature limit, or when the electronic coupling is small, the FCWD can be approximated as:

$$FCWD = \frac{1}{\sqrt{4\pi\lambda RT}} \exp\left(-\frac{(\Delta G + \lambda)^2}{4\pi\lambda RT}\right). \quad (7)$$

Here, λ is the reorganization energy, R the universal gas constant, T the temperature and ΔG the standard free energy difference. When taking the natural logarithm of both sides of Eq. (6) and inserting Eq. (7) into Eq. (6), one obtains a quadratic function in ΔG. This gives a downwards oriented parabola in which the width increases with a larger reorganization energy. This is further elaborated by Shuai et al., who applied the simple Marcus model to rationalize the effect of the total reorganization energies on the internal conversion rates.[81] For **1a**-**1e**, this energy gap dependence is shown in **Figure 5**. One can note that there is an almost linear relationship between the logarithm of $k_{ic,21}$ and the S_2-S_1 adiabatic energy gap for all azulene derivatives. However, when comparing **1a** and **1d**, or **1b** and **1e**, they have almost the same S_2-S_1 adiabatic energy gap, but still a significantly different rate. This originates from their different non-adiabatic couplings, which can ultimately be linked to their REs. In a nutshell, for **1a**-**1e**, their total REs dictate the non-radiative rates and hence their ϕ_{20} values. This is the ultimate reason for the violations of the energy gap law within the series of azulene derivatives.

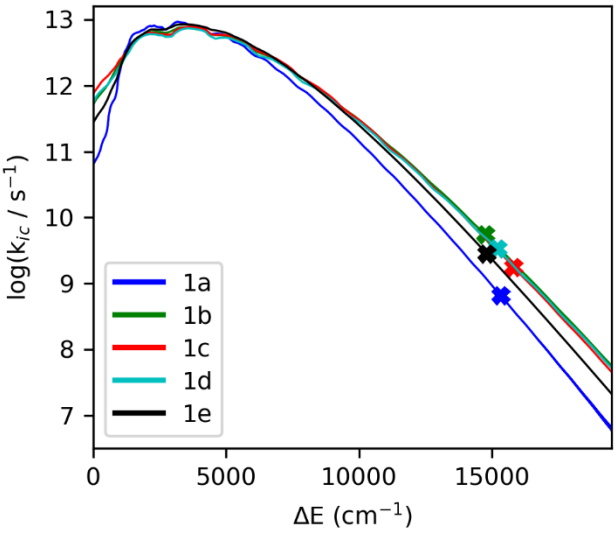

Figure 5. Logarithm of the $S_2 \rightarrow S_1$ internal conversion rate as a function of the S_2-S_1 adiabatic energy gap for **1a**-**1e**. The values marked with an **X** correspond to their computed S_2-S_1 adiabatic energy gaps.

Let us now investigate in more detail the accepting normal modes promoting the $S_2 \rightarrow S_1$ IC process. The reorganization energy λ_k from the kth normal mode is defined as the product of its corresponding Huang-Rhys factor, i.e., HR_k, times its energy $h\omega_k$; see Eq. (8).

$$\lambda_k = HR_k * \hbar\omega_k. \tag{8}$$

HR_k is a direct measurement of the extent of vibronic coupling between the two electronic states. In addition, the total reorganization energies are defined as:

$$\lambda_{tot} = \sum_{k=1}^{3n-6} \lambda_k. \tag{9}$$

Figure 6 shows the results of the electron-vibrational coupling calculations for the $S_2 \rightarrow S_1$ IC process. More in detail, the REs for each vibrational mode, and the total REs are shown in **Figure 6** (for the total REs of the $S_2 \rightarrow S_0$ and $S_1 \rightarrow S_0$ IC processes see **Table S4**). It can be seen that the

unsubstituted azulene (**1a**) and the *5,6*-disubstituted compound (**1e**) possess very similar patterns, and that is also the case for the *1,3*-disubstituted compounds (**1c-d**).

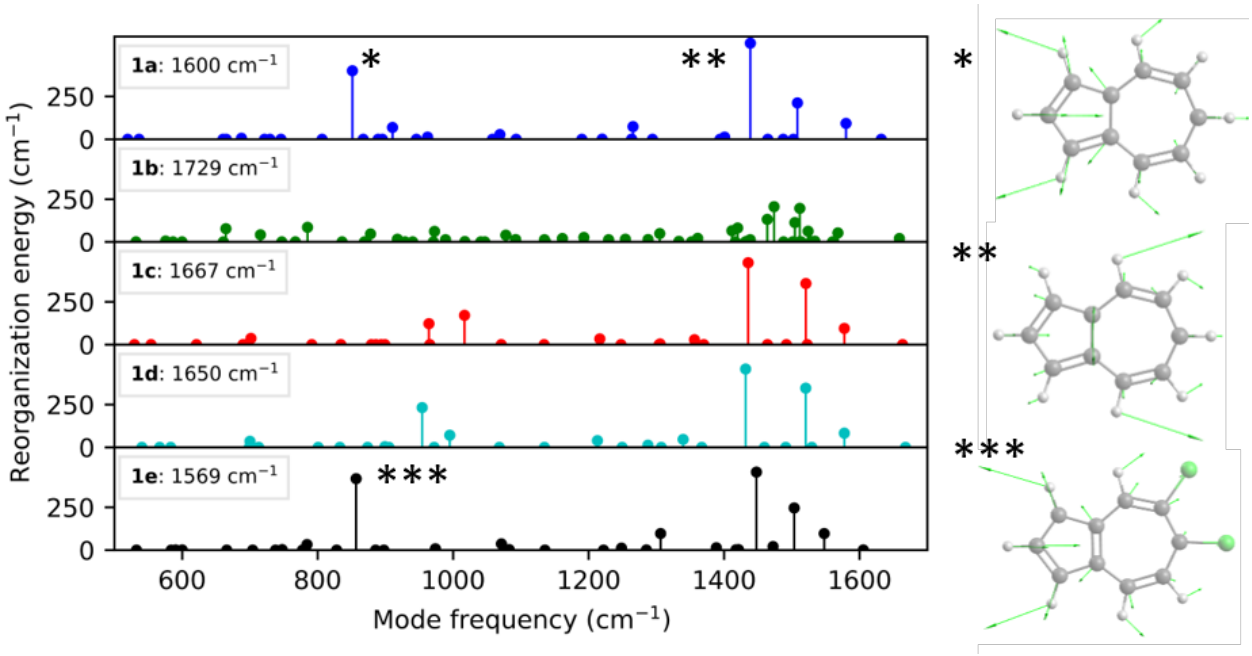

Figure 6. Reorganization energies for the different modes of molecules **1a** (top) to **1e** (bottom), together with their total REs for the $S_2 \rightarrow S_1$ IC process, shown in the top-left corner. Relevant accepting modes with high REs are highlighted and shown on the right panel.

The first thing to note is that **1a** and **1e** possess the lowest total REs (1601 and 1569 cm^{-1}, respectively). Conversely, **1b-d** possess ca. 100 cm^{-1} larger REs than **1a-e**. This correlates well with the computed larger $k_{ic,21}$ values for the former compounds (see **Table 2**). Another peculiarity of compounds **1a-e** is the presence of a low frequency mode at ca. 850 cm^{-1} characterized by a large reorganization energy. This accepting mode mainly corresponds to the bending of the hydrogen atoms situated at the *1,3* positions (see **Figure 6**). Conversely, for **1b**, **1c** and **1d**, the presence of heavy-atom substituents at the *1,3* positions blocks this low frequency accepting mode and thus a smaller reorganization energy is obtained in this case. Certainly, the presence of this intense low frequency mode for **1a** and **1e** could indicate a stronger dependency with temperature

for their $k_{ic,21}$ values, especially at the low temperature regime. At the higher frequency regime, all the azulene derivatives except **1b** possess their most relevant accepting mode at ca. 1450 cm^{-1}. This accepting mode corresponds to the C9-C10 stretching with contributions from the bending of hydrogens located at the 4,8 positions (see **Figure 6**). The relevance of this accepting mode is in line with our expectations because the main geometrical changes during the decay from S_2 to S_1 is the shortening of the middle C-C bond, and hence highlighting the importance of this central stretching mode.

Finally, a discussion of the computed fluorescence quantum yields follows. Importantly, despite the difficulties in calculating photoluminescence quantum yields in an accurate manner (see discussion above), we note a satisfactory agreement between the computed and the experimental data. First, the computed ϕ_{20} values with Eq. (2) for **1a**-**e** are of the same order of magnitude as the experimental ones (i.e., values between ca. 0.5-5%, see Table 2). We remark that we are also able recover some of the experimental trends, note for instance that compounds **1a,c** possess both the largest calculated and measured ϕ_{20} values. This can be considered as a success having in mind the small variability between the ϕ_{20} values within the series of azulene derivatives along with the difficulties in accurately predicting fluorescence quantum yields at the first principles level. In addition, the ϕ_{10} values were also computed using Eq. (5). For the $S_1 \rightarrow S_0$ transitions, their radiative rates are about ten times smaller than the $k_{r,20}$ values (compare in **Table 2**), which makes the latter radiative rates competitive with $k_{ic,21}$. All these factors along with the larger $k_{ic,10}$ values than the $k_{r,10}$ ones, contribute to the negligible ϕ_{10} values. In a nutshell, the anti-Kasha behavior for the azulene derivatives can be unambiguously predicted using our herein developed computational protocol. We foresee the validity of this protocol to predict other non-thermally equilibrated anti-Kasha emissions (or dual emissive scenarios) involving S_2 (or S_n) and S_1.

CONCLUSION

Since Kasha's and Turro's (among others) early discoveries during the period between the 50's-70's on molecular systems violating Kasha's rule, i.e., "polyatomic molecular entities react with appreciable yield only from the lowest excited state of a given multiplicity", more and more molecular systems have been proven to display anomalous anti-Kasha emissions. The observation of anti-Kasha photochemical processes is ultimately controlled by kinetic factors. An in-depth analysis and rationalization of anti-Kasha photochemical events is not only relevant from a fundamental viewpoint but it may also lead to potential technological breakthroughs to e.g., efficiently harness the excess of electronic energy in optoelectronics, photovoltaic devices and/or artificial photosynthesis. In addition, new technological advances in optical imaging and sensing can be derived from the external stimuli-dependent (i.e., excitation wavelength-dependent) emissive properties of anti-Kasha behaving molecular systems. In this regard, computational investigations are very valuable tools for understanding (firstly) and controlling (secondly) anti-Kasha photochemical events. In this manuscript, we present, for the first time, a computational protocol to predict anti-Kasha photoluminescence in molecular systems by combining: quantum chemical calculations, diverse excited state decay rate theories and appropriate kinetic models. The validity of this computational protocol for a series of azulene derivatives (i.e., non-thermally equilibrated anti-Kasha case) has been verified. As an outlook we are currently extending the current protocols to cover also thermally-equilibrated anti-Kasha events.

ASSOCIATED CONTENT

Supporting Information.

The supporting information contains the following data: extra computational details, main geometrical parameters of the optimized geometries, frontier molecular orbital plots, electron density difference plots, radiative and non-radiative rates, reorganization energies and xyz-coordinates of the optimized geometries.

AUTHOR INFORMATION

Corresponding Author

*Daniel Escudero. E-mail: Daniel.escudero@kuleuven.be

Author Contributions

K. V.: Investigation, Formal analysis, Writing - review & editing. D. E.: Conceptualization, Formal analysis, Writing - review & editing, Funding acquisition. All authors have given approval to the final version of the manuscript.

Funding Sources

D. E. acknowledges KU Leuven internal funds.

ACKNOWLEDGMENT

D. E. acknowledges KU Leuven internal funds.

REFERENCES

(1) Kasha, M. Characterization of Electronic Transitions in Complex Molecules. *Discuss. Faraday Soc.* **1950**, *9* (c), 14. https://doi.org/10.1039/df9500900014.

(2) IUPAC. Isotopomer. In *IUPAC Compendium of Chemical Terminology*; IUPAC: Research

Triagle Park, NC, **2014**. https://doi.org/10.1351/goldbook.I03352.

(3) Braslavsky, S. E. Glossary of Terms Used in Photochemistry, 3rd Edition (IUPAC Recommendations 2006). *Pure Appl. Chem.* **2007**, *79* (3), 293–465. https://doi.org/10.1351/pac200779030293.

(4) Demchenko, A. P.; Tomin, V. I.; Chou, P.-T. Breaking the Kasha Rule for More Efficient Photochemistry. *Chem. Rev.* **2017**, *117* (21), 13353–13381. https://doi.org/10.1021/acs.chemrev.7b00110.

(5) Röhrs, M.; Escudero, D. Multiple Anti-Kasha Emissions in Transition-Metal Complexes. *J. Phys. Chem. Lett.* **2019**, *10* (19), 5798–5804. https://doi.org/10.1021/acs.jpclett.9b02477.

(6) Escudero, D.; Thiel, W. Exploring the Triplet Excited State Potential Energy Surfaces of a Cyclometalated Pt(II) Complex: Is There Non-Kasha Emissive Behavior? *Inorg. Chem.* **2014**, *53* (20), 11015–11019. https://doi.org/10.1021/ic501430x.

(7) Viswanath, G.; Kasha, M. Confirmation of the Anomalous Fluorescence of Azulene. *J. Chem. Phys.* **1956**, *24* (3), 574–577. https://doi.org/10.1063/1.1742548.

(8) Turro, N. J.; Ramamurthy, V.; Cherry, W.; Farneth, W. The Effect of Wavelength on Organic Photoreactions in Solution. Reactions from Upper Excited States. *Chem. Rev.* **1978**, *78* (2), 125–145. https://doi.org/10.1021/cr60312a003.

(9) Itoh, T. Fluorescence and Phosphorescence from Higher Excited States of Organic Molecules. *Chem. Rev.* **2012**, *112* (8), 4541–4568. https://doi.org/10.1021/cr200166m.

(10) Tomin, V. I.; Dubrovkin, J. M. Kinetics of Anti-Kasha Photoreactions. Direct Excitation of a Higher Excited State. *ChemistrySelect* **2017**, *2* (27), 8354–8361. https://doi.org/10.1002/slct.201701518.

(11) Itoh, T. Evidence for the Coexistence of Two Different Mechanisms for the Occurrence of

Anti-Kasha S2 (1 1Bu) Fluorescence from α,ω-Diphenylpolyenes. *J. Chem. Phys.* **2004**, *121* (14), 6956–6960. https://doi.org/10.1063/1.1791155.

(12) Kumar, S.; Hisamatsu, Y.; Tamaki, Y.; Ishitani, O.; Aoki, S. Design and Synthesis of Heteroleptic Cyclometalated Iridium(III) Complexes Containing Quinoline-Type Ligands That Exhibit Dual Phosphorescence. *Inorg. Chem.* **2016**, *55* (8), 3829–3843. https://doi.org/10.1021/acs.inorgchem.5b02872.

(13) He, Z.; Zhao, W.; Lam, J. W. Y.; Peng, Q.; Ma, H.; Liang, G.; Shuai, Z.; Tang, B. Z. White Light Emission from a Single Organic Molecule with Dual Phosphorescence at Room Temperature. *Nat. Commun.* **2017**, *8* (1), 416. https://doi.org/10.1038/s41467-017-00362-5.

(14) Yeh, Y.-S.; Cheng, Y.-M.; Chou, P.-T.; Lee, G.-H.; Yang, C.-H.; Chi, Y.; Shu, C.-F.; Wang, C.-H. A New Family of Homoleptic Ir(III) Complexes: Tris-Pyridyl Azolate Derivatives with Dual Phosphorescence. *ChemPhysChem* **2006**, *7* (11), 2294–2297. https://doi.org/10.1002/cphc.200600461.

(15) Brancato, G.; Signore, G.; Neyroz, P.; Polli, D.; Cerullo, G.; Abbandonato, G.; Nucara, L.; Barone, V.; Beltram, F.; Bizzarri, R. Dual Fluorescence through Kasha's Rule Breaking: An Unconventional Photomechanism for Intracellular Probe Design. *J. Phys. Chem. B* **2015**, *119* (20), 6144–6154. https://doi.org/10.1021/acs.jpcb.5b01119.

(16) Zhou, Y.; Baryshnikov, G.; Li, X.; Zhu, M.; Ågren, H.; Zhu, L. Anti-Kasha's Rule Emissive Switching Induced by Intermolecular H-Bonding. *Chem. Mater.* **2018**, *30* (21), 8008–8016. https://doi.org/10.1021/acs.chemmater.8b03699.

(17) del Valle, J. C.; Catalán, J. Kasha's Rule: A Reappraisal. *Phys. Chem. Chem. Phys.* **2019**, *21* (19), 10061–10069. https://doi.org/10.1039/C9CP00739C.

(18) Jacquemin, D.; Escudero, D. Thermal Equilibration between Excited States or Solvent Effects: Unveiling the Origins of Anomalous Emissions in Heteroleptic Ru(Ii) Complexes. *Phys. Chem. Chem. Phys.* **2018**, *20*, 11559-11563. https://doi.org/10.1039/c8cp01101j.

(19) Crespo-Otero, R.; Barbatti, M. Recent Advances and Perspectives on Nonadiabatic Mixed Quantum-Classical Dynamics. *Chemical Reviews*. **2018**, *118*, (15), 7026-7068. https://doi.org/10.1021/acs.chemrev.7b00577.

(20) Zhang, X.; Jacquemin, D.; Peng, Q.; Shuai, Z.; Escudero, D. General Approach To Compute Phosphorescent OLED Efficiency. *J. Phys. Chem. C* **2018**, *122* (11), 6340–6347. https://doi.org/10.1021/acs.jpcc.8b00831.

(21) Niu, Y.; Peng, Q.; Deng, C.; Gao, X.; Shuai, Z. Theory of Excited State Decays and Optical Spectra: Application to Polyatomic Molecules. *J. Phys. Chem. A* **2010**, *114* (30), 7817–7831. https://doi.org/10.1021/jp101568f.

(22) Li, H.; Wang, X.; Zhu, Y.; Li, Z. Innovative Organic Electroluminescent Materials with a Doublet Ground State: A Theoretical Investigation. *J. Phys. Chem. A* **2020**, *124* (4), 662–673. https://doi.org/10.1021/acs.jpca.9b10343.

(23) Deng, C.; Niu, Y.; Peng, Q.; Qin, A.; Shuai, Z.; Tang, B. Z. Theoretical Study of Radiative and Non-Radiative Decay Processes in Pyrazine Derivatives. *J. Chem. Phys.* **2011**, *135* (1), 014304. https://doi.org/10.1063/1.3606579.

(24) Zhang, T.; Zhu, G.; Lin, L.; Mu, J.; Ai, B.; Li, Y.; Zhuo, S. Cyano Substitution Effect on the Emission Quantum Efficiency in Stilbene Derivatives: A Computational Study. *Org. Electron.* **2019**, *68*, 264–270. https://doi.org/10.1016/j.orgel.2019.01.049.

(25) Lv, L.; Yuan, K.; Zhu, Y.; Zuo, G.; Wang, Y. Investigation of Conversion and Decay Processes in Thermally Activated Delayed Fluorescence Copper(I) Molecular Crystal:

Theoretical Estimations from an ONIOM Approach Combined with the Tuned Range-Separated Density Functional Theory. *J. Phys. Chem. A* **2019**, *123* (10), 2080–2090. https://doi.org/10.1021/acs.jpca.9b00321.

(26) Lv, L.; Yuan, K.; Si, C.; Zuo, G.; Wang, Y. Mechanism Study of TADF and Phosphorescence in Dinuclear Copper (I) Molecular Crystal Using QM/MM Combined with an Optimally Tuned Range-Separated Hybrid Functional. *Org. Electron.* **2020**, *81* (December 2019), 105667. https://doi.org/10.1016/j.orgel.2020.105667.

(27) Shi, L.; Yan, C.; Guo, Z.; Chi, W.; Wei, J.; Liu, W.; Liu, X.; Tian, H.; Zhu, W.-H. De Novo Strategy with Engineering Anti-Kasha/Kasha Fluorophores Enables Reliable Ratiometric Quantification of Biomolecules. *Nat. Commun.* **2020**, *11* (1), 793. https://doi.org/10.1038/s41467-020-14615-3.

(28) Gong, Y.; Zhou, Y.; Yue, B.; Wu, B.; Sun, R.; Qu, S.; Zhu, L. Multiwavelength Anti-Kasha's Rule Emission on Self-Assembly of Azulene-Functionalized Persulfurated Arene. *J. Phys. Chem. C* **2019**, *123* (36), 22511–22518. https://doi.org/10.1021/acs.jpcc.9b06731.

(29) Blice-Baum, A.; Van Dyke, A.; Sigmon, I.; Salter, E. A.; Wierzbicki, A.; Pocker, Y.; Spyridis, G. T. Computational and Spectroscopic Studies Concerning the Solvatochromic Behavior of 1,3-Disubstituted Azulenes. *Int. J. Quantum Chem.* **2006**, *106* (11), 2331–2338. https://doi.org/10.1002/qua.20989.

(30) Xia, J.; Capozzi, B.; Wei, S.; Strange, M.; Batra, A.; Moreno, J. R.; Amir, R. J.; Amir, E.; Solomon, G. C.; Venkataraman, L.; et al. Breakdown of Interference Rules in Azulene, a Nonalternant Hydrocarbon. *Nano Lett.* **2014**, *14* (5), 2941–2945. https://doi.org/10.1021/nl5010702.

(31) Xin, H.; Gao, X. Application of Azulene in Constructing Organic Optoelectronic Materials:

New Tricks for an Old Dog. *Chempluschem* **2017**, *82* (7), 945–956. https://doi.org/10.1002/cplu.201700039.

(32) Yamaguchi, Y.; Ogawa, K.; Nakayama, K.; Ohba, Y.; Katagiri, H. Terazulene: A High-Performance n-Type Organic Field-Effect Transistor Based on Molecular Orbital Distribution Control. *J. Am. Chem. Soc.* **2013**, *135* (51), 19095–19098. https://doi.org/10.1021/ja410696j.

(33) Murata, S.; Iwanaga, C.; Toda, T.; Kokubun, H. Fluorescence and Radiationless Transitions from the Second Excited States of Azulene Derivatives. *Berichte der Bunsengesellschaft für Phys. Chemie* **1972**, *76* (11), 1176–1183. https://doi.org/10.1002/bbpc.19720761110.

(34) Griesser, H. J.; Wild, U. P. The Energy Gap Dependence of the Radiationless Transition Rates in Azulene and Its Derivatives. *Chem. Phys.* **1980**, *52* (1–2), 117–131. https://doi.org/10.1016/0301-0104(80)85190-1.

(35) Salahub, D. R.; Zerner, M. C. ChemInform Abstract: The Challenge of d and f Electrons. Theory and Computation. *ChemInform* **1990**. https://doi.org/10.1002/chin.199033368.

(36) Hohenberg, P.; Kohn, W. Inhomogeneous Electron Gas. *Phys. Rev.* **1964**, *136*, B864-B871. https://doi.org/10.1103/PhysRev.136.B864.

(37) Kohn, W.; Sham, L. J. Self-Consistent Equations Including Exchange and Correlation Effects. *Phys. Rev.* **1965**, *140*, A1133-A1138. https://doi.org/10.1103/PhysRev.140.A1133.

(38) Casida, M. E. Time-Dependent Density Functional Response Theory for Molecules; **1995**, 155–192. https://doi.org/10.1142/9789812830586_0005.

(39) Runge, E.; Gross, E. K. U. Density-Functional Theory for Time-Dependent Systems. *Phys. Rev. Lett.* **1984**, *52* (12), 997–1000. https://doi.org/10.1103/PhysRevLett.52.997.

(40) Adamo, C.; Barone, V. Toward Reliable Density Functional Methods without Adjustable

Parameters: The PBE0 Model. *J. Chem. Phys.* **1999**, *110*, 6158. https://doi.org/10.1063/1.478522.

(41) Perdew, J. P.; Burke, K.; Ernzerhof, M. Generalized Gradient Approximation Made Simple. *Phys. Rev. Lett.* **1996**, *77*, 3865. https://doi.org/10.1103/PhysRevLett.77.3865.

(42) Perdew, J. P.; Burke, K.; Ernzerhof, M. Erratum: Generalized Gradient Approximation Made Simple (Physical Review Letters (1996) 77 (3865)). *Physical Review Letters*. **1997**, *78*, 1396. https://doi.org/10.1103/PhysRevLett.78.1396.

(43) Ditchfield, R.; Hehre, W. J.; Pople, J. A. Self- Consistent Molecular- Orbital Methods. IX. An Extended Gaussian- Type Basis for Molecular- Orbital Studies of Organic Molecules. *J. Chem. Phys.* **1971**, *54* (2), 724–728. https://doi.org/10.1063/1.1674902.

(44) Hehre, W. J.; Ditchfield, R.; Pople, J. A. Self—Consistent Molecular Orbital Methods. XII. Further Extensions of Gaussian—Type Basis Sets for Use in Molecular Orbital Studies of Organic Molecules. *J. Chem. Phys.* **1972**, *56* (5), 2257–2261. https://doi.org/10.1063/1.1677527.

(45) Hariharan, P. C.; Pople, J. A. The Influence of Polarization Functions on Molecular Orbital Hydrogenation Energies. *Theor. Chim. Acta* **1973**, *28* (3), 213–222. https://doi.org/10.1007/BF00533485.

(46) Hariharan, P. C.; Pople, J. A. Accuracy of AH n Equilibrium Geometries by Single Determinant Molecular Orbital Theory. *Mol. Phys.* **1974**, *27* (1), 209–214. https://doi.org/10.1080/00268977400100171.

(47) Gordon, M. S. The Isomers of Silacyclopropane. *Chem. Phys. Lett.* **1980**, *76* (1), 163–168. https://doi.org/10.1016/0009-2614(80)80628-2.

(48) Francl, M. M.; Pietro, W. J.; Hehre, W. J.; Binkley, J. S.; Gordon, M. S.; DeFrees, D. J.;

Pople, J. A. Self- consistent Molecular Orbital Methods. XXIII. A Polarization- type Basis Set for Second- row Elements. *J. Chem. Phys.* **1982**, *77* (7), 3654–3665. https://doi.org/10.1063/1.444267.

(49) Binning, R. C.; Curtiss, L. A. Compact Contracted Basis Sets for Third-Row Atoms: Ga-Kr. *J. Comput. Chem.* **1990**, *11* (10), 1206–1216. https://doi.org/10.1002/jcc.540111013.

(50) Rassolov, V. A.; Pople, J. A.; Ratner, M. A.; Windus, T. L. 6-31G * Basis Set for Atoms K through Zn. *J. Chem. Phys.* **1998**, *109* (4), 1223–1229. https://doi.org/10.1063/1.476673.

(51) Rassolov, V. A.; Ratner, M. A.; Pople, J. A.; Redfern, P. C.; Curtiss, L. A. 6-31G* Basis Set for Third-Row Atoms. *J. Comput. Chem.* **2001**, *22* (9), 976–984. https://doi.org/10.1002/jcc.1058.

(52) Blaudeau, J.-P.; McGrath, M. P.; Curtiss, L. A.; Radom, L. Extension of Gaussian-2 (G2) Theory to Molecules Containing Third-Row Atoms K and Ca. *J. Chem. Phys.* **1997**, *107* (13), 5016–5021. https://doi.org/10.1063/1.474865.

(53) Dreuw, A.; Wormit, M. The Algebraic Diagrammatic Construction Scheme for the Polarization Propagator for the Calculation of Excited States. *Wiley Interdiscip. Rev. Comput. Mol. Sci.* **2015**, *5* (1), 82–95. https://doi.org/10.1002/wcms.1206.

(54) Weigend, F.; Häser, M.; Patzelt, H.; Ahlrichs, R. RI-MP2: Optimized Auxiliary Basis Sets and Demonstration of Efficiency. *Chem. Phys. Lett.* **1998**, *294* (1–3), 143–152. https://doi.org/10.1016/S0009-2614(98)00862-8.

(55) Jacquemin, D. Excited-State Dipole and Quadrupole Moments: TD-DFT versus CC2. *J. Chem. Theory Comput.* **2016**, *12* (8), 3993–4003. https://doi.org/10.1021/acs.jctc.6b00498.

(56) Niu, Y.; Li, W.; Peng, Q.; Geng, H.; Yi, Y.; Wang, L.; Nan, G.; Wang, D.; Shuai, Z. MOlecular MAterials Property Prediction Package (MOMAP) 1.0: A Software Package for

Predicting the Luminescent Properties and Mobility of Organic Functional Materials. *Mol. Phys.* **2018**, *116* (7–8), 1078–1090. https://doi.org/10.1080/00268976.2017.1402966.

(57) Niu, Y.; Peng, Q.; Shuai, Z. Promoting-Mode Free Formalism for Excited State Radiationless Decay Process with Duschinsky Rotation Effect. *Sci. China Ser. B Chem.* **2008**, *51* (12), 1153–1158. https://doi.org/10.1007/s11426-008-0130-4.

(58) Peng, Q.; Yi, Y.; Shuai, Z.; Shao, J. Toward Quantitative Prediction of Molecular Fluorescence Quantum Efficiency: Role of Duschinsky Rotation. *J. Am. Chem. Soc.* **2007**, *129* (30), 9333–9339. https://doi.org/10.1021/ja067946e.

(59) Parker, S. M.; Rappoport, D.; Furche, F. Quadratic Response Properties from TDDFT: Trials and Tribulations. *J. Chem. Theory Comput.* **2018**, *14* (2), 807–819. https://doi.org/10.1021/acs.jctc.7b01008.

(60) Yanai, T.; Tew, D. P.; Handy, N. C. A New Hybrid Exchange–Correlation Functional Using the Coulomb-Attenuating Method (CAM-B3LYP). *Chem. Phys. Lett.* **2004**, *393* (1–3), 51–57. https://doi.org/10.1016/j.cplett.2004.06.011.

(61) Dunning, T. H. Gaussian Basis Sets for Use in Correlated Molecular Calculations. I. The Atoms Boron through Neon and Hydrogen. *J. Chem. Phys.* **1989**, *90* (2), 1007–1023. https://doi.org/10.1063/1.456153.

(62) Kendall, R. A.; Dunning, T. H.; Harrison, R. J. Electron Affinities of the First- row Atoms Revisited. Systematic Basis Sets and Wave Functions. *J. Chem. Phys.* **1992**, *96* (9), 6796–6806. https://doi.org/10.1063/1.462569.

(63) Woon, D. E.; Dunning, T. H. Gaussian Basis Sets for Use in Correlated Molecular Calculations. III. The Atoms Aluminum through Argon. *J. Chem. Phys.* **1993**, *98* (2), 1358–1371. https://doi.org/10.1063/1.464303.

(64) Woon, D. E.; Dunning, T. H. Gaussian Basis Sets for Use in Correlated Molecular Calculations. IV. Calculation of Static Electrical Response Properties. *J. Chem. Phys.* **1994**, *100* (4), 2975–2988. https://doi.org/10.1063/1.466439.

(65) Foresman, J. B.; Head-Gordon, M.; Pople, J. A.; Frisch, M. J. Toward a Systematic Molecular Orbital Theory for Excited States. *J. Phys. Chem.* **1992**, *96* (1), 135–149. https://doi.org/10.1021/j100180a030.

(66) Frisch G. W.; Schlegel, H. B.; Scuseria, G. E.; Robb, M. A.; Cheeseman, J. R.; Scalmani, G.; Barone, V.; Petersson, G. A.; Nakatsuji, H.; Li, X.; Caricato, M.; Marenich, A. V.; Bloino, J.; Janesko, B. G.; Gomperts, R.; Mennucci, B.; Hratch, D. J., M. J. . T. Gaussian 16, Rev. A.03. *Gaussian, Inc., Wallingford, CT* **2016**. https://doi.org/111.

(67) Trofimov, A. B.; Schirmer, J. An Efficient Polarization Propagator Approach to Valence Electron Excitation Spectra. *J. Phys. B At. Mol. Opt. Phys.* **1995**, *28* (12) 2299-2324. https://doi.org/10.1088/0953-4075/28/12/003.

(68) Hättig, C.; Köhn, A. Transition Moments and Excited-State First-Order Properties in the Coupled-Cluster Model CC2 Using the Resolution-of-the-Identity Approximation. *J. Chem. Phys.* **2002**, *117* (15), 6939–6951. https://doi.org/10.1063/1.1506918.

(69) Sokolov, A. Y. Multi-Reference Algebraic Diagrammatic Construction Theory for Excited States: General Formulation and First-Order Implementation. *J. Chem. Phys.* **2018**, *149* (20), 204113. https://doi.org/10.1063/1.5055380.

(70) TURBOMOLE V7.1 2016, a Development of University of Karlsruhe and Forschungszentrum Karlsruhe GmbH, 1989-2007, TURBOMOLE GmbH, since 2007; Available from http://www.turbomole.com.

(71) Aidas, K.; Angeli, C.; Bak, K. L.; Bakken, V.; Bast, R.; Boman, L.; Christiansen, O.;

Cimiraglia, R.; Coriani, S.; Dahle, P.; et al. The Dalton Quantum Chemistry Program System. *Wiley Interdiscip. Rev. Comput. Mol. Sci.* **2014**, *4* (3), 269–284. https://doi.org/10.1002/wcms.1172.

(72) Dalton, a Molecular Electronic Structure Program, Release V2016.2 (2017), See http://daltonprogram.org.

(73) Loos, P. F.; Lipparini, F.; Boggio-Pasqua, M.; Scemama, A.; Jacquemin, D. A Mountaineering Strategy to Excited States: Highly Accurate Energies and Benchmarks for Medium Sized Molecules. *J. Chem. Theory Comput.* **2020**, *16* (3) 1711-1741. https://doi.org/10.1021/acs.jctc.9b01216.

(74) Murakami, A.; Kobayashi, T.; Goldberg, A.; Nakamura, S. CASSCF and CASPT2 Studies on the Structures, Transition Energies, and Dipole Moments of Ground and Excited States for Azulene. *J. Chem. Phys.* **2004**, *120* (3), 1245–1252. https://doi.org/10.1063/1.1631914.

(75) Krykunov, M.; Grimme, S.; Ziegler, T. Accurate Theoretical Description of the 1 L a and 1 L b Excited States in Acenes Using the All Order Constricted Variational Density Functional Theory Method and the Local Density Approximation. *J. Chem. Theory Comput.* **2012**, *8* (11), 4434–4440. https://doi.org/10.1021/ct300372x.

(76) Shevyakov, S. V.; Li, H.; Muthyala, R.; Asato, A. E.; Croney, J. C.; Jameson, D. M.; Liu, R. S. H. H. Orbital Control of the Color and Excited State Properties of Formylated and Fluorinated Derivatives of Azulene †. *J. Phys. Chem. A* **2003**, *107* (18), 3295–3299. https://doi.org/10.1021/jp021605f.

(77) Prlj, A.; Begušić, T.; Zhang, Z. T.; Fish, G. C.; Wehrle, M.; Zimmermann, T.; Choi, S.; Roulet, J.; Moser, J.-E.; Vaníček, J. Semiclassical Approach to Photophysics Beyond Kasha's Rule and Vibronic Spectroscopy Beyond the Condon Approximation. The Case of

Azulene. *J. Chem. Theory Comput.* **2020**, *16* (4), 2617–2626. https://doi.org/10.1021/acs.jctc.0c00079.

(78) Woudenberg, T. M.; Kulkarni, S. K.; Kenny, J. E. Internal Conversion Rates for Single Vibronic Levels of S 2 in Azulene. *J. Chem. Phys.* **1988**, *89* (5), 2789–2796. https://doi.org/10.1063/1.455032.

(79) Peng, Q.; Shi, Q.; Niu, Y.; Yi, Y.; Sun, S.; Li, W.; Shuai, Z. Understanding the Efficiency Drooping of the Deep Blue Organometallic Phosphors: A Computational Study of Radiative and Non-Radiative Decay Rates for Triplets. *J. Mater. Chem. C* **2016**, *4* (28), 6829–6838. https://doi.org/10.1039/c6tc00858e.

(80) Balzani, V.; Juris, A.; Venturi, M.; Campagna, S.; Serroni, S. Luminescent and Redox-Active Polynuclear Transition Metal Complexes †. *Chem. Rev.* **1996**, *96* (2), 759–834. https://doi.org/10.1021/cr941154y.

(81) Shuai, Z.; Peng, Q. Excited States Structure and Processes: Understanding Organic Light-Emitting Diodes at the Molecular Level. *Phys. Rep.* **2014**, *537* (4), 123–156. https://doi.org/10.1016/j.physrep.2013.12.002.

TOC graphic

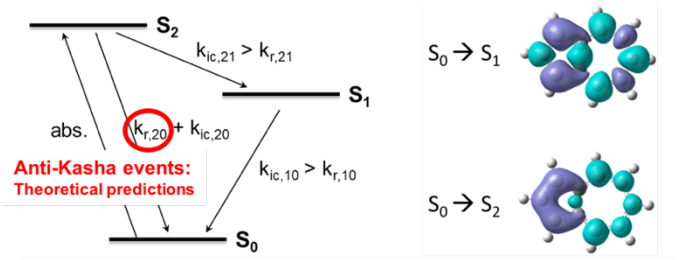
S2
kic,21 > kr,21
S1
abs.
kr,20 + kic,20
Anti-Kasha events:
Theoretical predictions
kic,10 > kr,10
S0
S0 → S1
S0 → S2

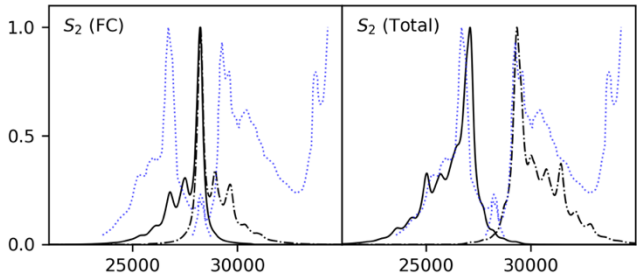
S2 (FC)
S2 (Total)
1.0
0.5
0.0
25000
30000
25000
30000